water

MDPI

Article

Aqueous-Medium Arsenic(V) Removal Using Iron Oxide-Coated Ignimbrite

Leslie Diana Velarde-Apaza [1,2], Azucena Chávez-Collantes [1], Richard Solorzano-Acosta [3,*], Juan-Pablo Cuevas [1] and José Antonio Villanueva-Salas [2]

[1] Dirección de Supervisión y Monitoreo en las Estaciones Experimentales, Estación Experimental Agraria de Baños del Inca, Instituto Nacional de Innovación Agraria (INIA), Jr. Wiracocha S/N, Baños del Inca, Cajamarca 06004, Peru; leslievelarde03@gmail.com (L.D.V.-A.); achavezc22@gmail.com (A.C.-C.); jcuevas@unc.edu.pe (J.-P.C.)
[2] Escuela de Posgrado, Universidad Católica de Santa Maria, Urb. San José, San Jose s/n, Yanahuara, Arequipa 04017, Peru; jvillans@ucsm.edu.pe
[3] Dirección de Supervisión y Monitoreo en las Estaciones Experimentales Agrarias, Instituto Nacional de Innovación Agraria (INIA), Av. La Molina 1981, Lima 15024, Peru
* Correspondence: investigacion_labsaf@inia.gob.pe

Abstract: Arsenate As(V) is a toxic contaminant commonly found in aquifers and groundwater that poses significant risks to human health. The effective treatment of arsenic-contaminated water is therefore crucial for safeguarding public health. This study investigates removing As(V) using iron oxide-coated ignimbrite in batch experiments by varying the adsorbent dosage, initial As(V) concentration, contact time, and system temperature. The adsorption experiments revealed that the Langmuir isotherm model better fit the data (R^2 = 0.99) than the Freundlich model (R^2 = 0.73). According to the Langmuir model, the maximum adsorption capacity of As(V) on the iron oxide-coated ignimbrite was 4.84 mg·g^{-1} ± 0.12 mg·g^{-1} of As(V), with a standard deviation of ±0.05 mg·g^{-1} after 2 h of exposure with 0.15 g/50 mL iron oxide-coated ignimbrite adsorbent concentration. In the kinetic analysis, the pseudo-first-order model best described the adsorption process at 283 K, 293 K, and 303 K, although the pseudo-second-order model also showed an adequate fit, particularly at 293 K. This indicates that, while the pseudo-first-order model is generally more suitable under these conditions, the pseudo-second-order model may also apply under certain circumstances. The results of the batch experiments demonstrate that iron oxide-coated ignimbrite is a promising adsorbent for effectively reducing high concentrations of As(V) in contaminated water.

Keywords: arsenic(V); ignimbrite; iron oxide; metal removal; adsorption; underground water

Academic Editor: Daniela Fighir

Received: 16 November 2024
Revised: 20 December 2024
Accepted: 21 December 2024
Published: 28 December 2024

Citation: Velarde-Apaza, L.D.; Chávez-Collantes, A.; Solorzano-Acosta, R.; Cuevas, J.-P.; Villanueva-Salas, J.A. Aqueous-Medium Arsenic(V) Removal Using Iron Oxide-Coated Ignimbrite. *Water* **2025**, *17*, 53. https://doi.org/10.3390/w17010053

1. Introduction

The heavy metal pollution of water bodies is a serious environmental problem on a global scale [1]. These metals, including lead, mercury, cadmium, and arsenic, have diverse origins in industry, mining, agriculture, and urban waste. They tend to accumulate in sediments and living organisms, which can have devastating consequences for aquatic systems, wildlife, and human health [2].

Aquifers and groundwater contamination by arsenic (As) has emerged as a concern in recent years due to its high toxicity and hazardousness to human health and the environment [3]. Arsenate As(V) is an inorganic form of arsenic (As) that can be incorporated into water bodies from natural sources and anthropogenic activities, such as mining and agriculture.

Chronic drinking water exposure to arsenate has been linked to cancer development [4,5] and neurological disorders [6,7]. Therefore, managing and reducing arsenate contamination is imperative to preserve the aquatic ecosystem's health and ensure a safe and sustainable water supply.

Several technologies based on coagulation/filtration, biological oxidation, electrochemical oxidation, and ion-exchange processes have been reported for removal from groundwater intended for human consumption [8–11]. However, further studies are needed to develop techniques that are accessible to the population and guarantee adequate water quality, which has made the use of pure or modified adsorbents an efficient tool for these purposes [12–14].

Adsorption technology utilizing iron oxide-coated ignimbrite for arsenic removal relies on the strong chemical affinity between the functional groups of iron oxide and arsenic ions, particularly arsenate As(V) ions. Iron oxide contains hydroxyl groups that can bind arsenic through surface complexation, where arsenate ions replace the hydroxyl groups on the iron oxide surface. This creates a stable bond that effectively removes arsenic from water, making it a highly efficient method for reducing arsenic contamination, as stated by Yılmaz et al. [15].

Regarding adsorption efficiency, two key factors are crucial: surface area and porosity. Adsorbents with a high surface area and porous structure, like ignimbrite, offer more active sites for binding arsenic ions, enhancing adsorption capacity. In addition, the material's surface modification is crucial, as the iron oxide coating significantly enhances the adsorptive properties of ignimbrite, increasing its selectivity for arsenic ions, particularly arsenate As(V). This modification improves the affinity for arsenic and influences adsorption kinetics, allowing faster ion exchange and maximum adsorption capacity, enabling the adsorbent to capture more significant amounts of arsenic. This makes the modified ignimbrite a highly effective material for arsenic removal in water treatment [16,17].

Adsorbents can trap and retain contaminants, such as As, through chemical or physical interactions. Pure adsorbents, such as iron oxide and activated carbon, are widely used for As removal in water treatment systems [14]. In addition, modified adsorbents, which have been specifically designed and treated to increase their adsorption capacity, can also work in As removal. These materials can be modified by metal oxide compounds, clays, and nanoparticles, which improve their efficiency and selectivity for arsenic capture [12]. In this way, these modified adsorbents can effectively address arsenic contamination in water supplies, ensuring safe drinking water and public health protection.

Ignimbrite is a volcanic stone of igneous origin with a white or cream color and porous texture. It has traditionally been used as a building material for its durability, strength, and distinctive aesthetics in the Arequipa region of southern Peru [18]. The mineralogical composition of this material has been reported by Lebti et al. [19]. In particular, La Joya ignimbrite is one of the most important outcrops in this region. It has the highest quartz (SiO_2) and sanidine ($KAlSi_3O_8$) content of all ignimbrites in Arequipa [19]. Due to its characteristics and properties, enhanced by its coating with iron oxides, it has been proposed as an adsorbent for contaminated water remediation by heavy metals.

Iron oxides, such as hematite, goethite, and magnetite, are widely used as effective adsorbents in heavy metal removal from polluted waters [13,20,21]. Iron oxides possess functional groups on their surface that can interact with metal ions, allowing chemical bond formation and metal retention in solution [22]. In addition, iron oxides are also attractive for these purposes due to their availability, affordability, and regenerative capacity, making them a sustainable option for heavy metal removal in water pollution management.

This research proposes using iron oxide-coated ignimbrite as an adsorbent material for As(V) removal in an aqueous solution to obtain an effective, accessible, and economical method for water purification intended for human consumption.

2. Materials and Methods

2.1. Ignimbrite Sampling

Ignimbrite samples were collected from a prominent natural outcrop in Arequipa, which has been used in construction and ornamentation for centuries [23,24]. The sampling point was located at the geographical coordinates 16°22′14.9″ S, 71°32′03.5″ W, at 2386 m.a.s.l. altitude, in the Chilina locality, Alto Selva Alegre district, on the Chili River's east bank.

2.2. Ignimbrite's Physicochemical Characterization and Mineralogical Composition

A 2 kg ignimbrite sample was characterized after being pulverized and sieved into 75 µm–150 µm, 150 µm–425 µm, and 425 µm–850 µm particles using USA Standard Testing Sieve ADVANTECH #200, #100, #40 y #20. Electrical conductivity (EC), pH, residual moisture, and organic matter content (OM) were determined by digital pH meter 827 pH lab, Metrohm®, Herisau, Switzerland, Conductometer SCHOTT Instruments handylab LF 11, Mainz, Germany and Muffle FB1300 Furnace Thermolyne™, Boston, MA, USA, respectively. In addition, elemental analysis by inductively coupled plasma optical emission spectroscopy (ICP–OES, Optima8000, Perkin Elmer, Waltham, MA, USA) was carried out to determine mineralogical composition and metal presence in ignimbrite.

2.3. Ignimbrite Modification by Coating with Iron Oxides

Ignimbrite's iron oxide coating was performed according to the procedure proposed by Thirunavukkarasu et al. [25], which consisted of a pre-conditioning and two coating stages. Conditioning consisted of immersing the ignimbrite in a 0.1 M nitric acid (Suprapur® MERCK®, Darmstadt, Germany) solution for 24 h. After a triple-rinse process with distilled water, the sample was dried at 383 K ± 1 K for 20 h by sterilization oven (UM-200, Memmert®, Schwabach, Germany).

In the initial stage of the coating process, 7.5 g of $Fe(NO_3)_3 \cdot 9H_2O$ (MERCK®, Germany) was dissolved in 25 mL of distilled water. Subsequently, 2.5 mL of 10 M NaOH (MERCK®, Germany) was added, and the mixture was continuously homogenized, forming a reddish-brown gelatinous precipitate that was indicative of $Fe(OH)_3$. The ignimbrite sample was then incorporated into the solution, and the mixture was homogenized for 10 min. The solution was heated for 4 h at 383 K ± 1 K, followed by an additional 3 h at 823 K ± 1 K by Magnetic stirrer with heating (Gallenkamp® Magnetic, London, UK). Finally, the mixture was allowed to cool to room temperature.

In the second phase of the process, 25 g of $Fe(NO_3)_3 \cdot 9H_2O$ (MERCK®, Germany) was dissolved in 22 mL of distilled water, and 5 mL of 10 M NaOH (MERCK®, Germany) was added. While homogenizing the mixture, the previously obtained solution (first stage of the coating process) was added, stirring constantly. The mixture was then heated to 383 K ± 1 K for 20 h. After cooling to room temperature, the new solution was mechanically disaggregated and sieved to obtain 150 µm–425 µm particles. After three repetitions of heating/cooling phases of 4 h at 383 K ± 1 K in each cycle, the solution was cooled for 20 h at room temperature.

2.4. Quantitative As(V) Analysis by Voltammetry

Voltammetry offers the ability to determine arsenic in its various forms, including arsenite As(III), total As, and As(V), by a potential difference [26]. However, since As(V) is electroinactive, a prior reduction of As(V) to As(III) is required to determine total As.

Sodium arsenate ($Na_2HAsO_4 \cdot 7H_2O$, MERCK®, Germany) solutions were used to reduce As(V) to As(III) and, therefore, to quantify the analyte in the samples. For this, 2 mL of 0.1 M L-cysteine solution (MERCK®, Germany) was used as the reducing agent, and 1 M HCl (MERCK®, Germany) was added to the sample, based on the procedure proposed by He et al. [27]. Then, the mixture was heated at 363 K ± 1 K for 10 min in a water bath to accelerate the reduction, avoiding sample loss by evaporation. Subsequently, the solution was cooled to room temperature, and the final volume was adjusted to 10 mL.

As(III) determination required the use of 1 M HCl (MERCK®, Germany) solution and the presence of Cu(II) (Standard Copper Solution, MERCK®, Germany) and Se(IV) (Standard Selenium Solution MERCK®, Germany) in the voltammetric cell (797 VA Computrace, Metrohm®, Switzerland) for proper analysis. The voltammetric technique needed to be validated through linearity, precision, accuracy, limit of detection, and limit of quantification parameters, as stated in USP 37 [28].

2.5. As(V) Removal by Iron Oxide-Coated Ignimbrite

Batch experiments were conducted to analyze sodium arsenate solutions at the beginning and end of the As(V) adsorption process using iron oxide-coated ignimbrite. A custom-made eight-station adsorption unit with thermoregulation, adapted from a German design, was used. The system operated within a temperature range of 10 to 40 °C, controlled by a hot/cold water bath system and a circulation pump. The rotary motion of the paddles was induced by a pulley system, with a speed range of 100–450 rpm.

Then, 50 mL of As(V) solution (from $Na_2HAsO_4 \cdot 7H_2O$, MERCK®, Germany) was mixed with the adsorbent (at different volumes) in 100 mL beakers, stirring constantly. Specific interval measurements were made and analyzed using voltammetry after centrifugation at 6000 rpm for 10 min. The adsorbed arsenic amount on the iron oxide-coated ignimbrite was calculated by comparing the initial concentrations and sample concentrations taken at different times according to the following equation:

$$q_t = (C_0 - C_t)\frac{V}{M} \quad (1)$$

Likewise, the adsorbed arsenic amount on the iron oxide coated ignimbrite at equilibrium was calculated with the following equation:

$$q_e = (C_0 - C_e)\frac{V}{M} \quad (2)$$

where q_e and q_t are the adsorption capacity of the metalloid at equilibrium and at a defined time (t), respectively ($mg \cdot g^{-1}$); C_0 is the initial concentration of arsenic ($mg \cdot L^{-1}$); C_e and C_t are the arsenic concentrations at equilibrium and at a defined time (t), respectively ($mg \cdot L^{-1}$); V is the solution volume (mL); and M is the adsorbent mass (g). Adsorption process efficiency was expressed in As(V) removal percentage, given by the following equation:

$$As(V)Removal\% = 100\% - \left(\frac{C_f}{C_0}100\%\right) \quad (3)$$

where C_f is the As(V) final concentration after contact time with the adsorbent and C_0 is the As(V) initial concentration. Both the As(V) removal percentage and the adsorption capacity

were calculated regarding four variables: adsorbent mass (g), As(V) initial concentration ($g \cdot L^{-1}$), contact time, and temperature.

2.6. Equilibrium Adsorption Study

Six different As(V) initial concentrations were evaluated between 1.31 and 32.72 $mg \cdot L^{-1}$. These solutions were prepared from a $Na_2HAsO_4 \cdot 7H_2O$ (MERCK®, Germany) stock solution dilution with a 2400 $mg \cdot L^{-1}$ As(V) concentration. A total of 47 mL of each As(V) solution mixed with 0.15 g ignimbrite was used, kept under constant stirring. Langmuir and Freundlich isotherm models were used to understand the adsorption mechanism and the arsenic-adsorbent interaction [27,29,30]. The following equation can describe the linear form of Langmuir's isotherm:

$$\frac{C_e}{q_e} = \frac{1}{K_L q_m} + \frac{1}{q_m} C_e \quad (4)$$

where q_e is the arsenic adsorption capacity at equilibrium ($mg \cdot g^{-1}$); C_e is As(V) concentration at equilibrium ($mg \cdot L^{-1}$); K_L is Langmuir's isotherm constant ($L \cdot mg^{-1}$), which is related to the adsorption free energy; and q_m is the maximum adsorption capacity ($mg \cdot g^{-1}$).

The following equation gives the linear form of Freundlich's isotherm:

$$log(q_e) = log\left(K_f\right) + \frac{1}{n} log(C_e) \quad (5)$$

where q_e is the arsenic adsorption capacity at equilibrium ($mg \cdot g^{-1}$); C_e is As(V) concentration at equilibrium ($mg \cdot L^{-1}$); K_f is Freundlich's isotherm constant, which is related with the adsorption process efficiency; and n is the heterogeneity factor, a dimensionless variable indicative of the adsorption process favorability. If the n value is 0–10, this indicates chemisorption [31].

The Langmuir model assumes homogeneous monolayer adsorption on the adsorbent surface with a finite number of identical interaction sites, while the Freundlich model is empirical and allows for multilayer adsorption [25].

2.7. As(V) Adsorption Kinetics

As(V) adsorption kinetics were evaluated at 283 K ± 1 K, 293 K ± 1 K, and 303 K ± 1 K. In experiments, 50 mL As(V) 15 $mg \cdot L^{-1}$ stock solution and 0.15 g iron oxide-coated ignimbrite were used. Readings were taken at different times for 140 min. To evaluate the adsorption process' kinetic order, pseudo-first-order and pseudo-second-order models were applied, whose equations are expressed in the linear form below.

Pseudo-first-order model:

$$\ln(q_e - q_t) = \ln(q_e) - k_1 t \quad (6)$$

where q_e and q_t are the adsorption capacities at equilibrium and at defined time t, respectively ($mg \cdot g^{-1}$), and $k_1 t$ is the pseudo-first-order adsorption rate constant ($1 \cdot min^{-1}$).

Pseudo-second-order model:

$$1/(q_e - q_t) = 1/q_e + k_2 t \quad (7)$$

where q_e and q_t are the adsorption capacities at equilibrium and at a defined time t, respectively ($mg \cdot g^{-1}$), and $k_2 t$ is the pseudo-second-order adsorption rate constant ($g \cdot mg\ min^{-1}$).

3. Results and Discussion

3.1. Ignimbrite's Physicochemical Properties and Mineral Composition

Ignimbrite's particles were 150–425 µm and showed a fine silty-sandy texture, whitish color, and very low solubility. Regarding chemical characteristics, its pH was 8.1, EC was 1.27 $dS{\cdot}m^{-1}$, residual humidity was 0.23% and OM was 0.33%. Carbonate presence is assumed due to the effervescence observed upon adding 0.1 M HCl.

Metal determination by ICP–OES showed the presence of 11 elements (Table 1). Na and K presented the highest concentration. Thus, some heavy metals (Ba, Cu, Fe, Mo, Sr, Ti) were also determined. Fe and Ti determination suggests the presence of these minerals' oxides.

Table 1. Identified metals present in the uncoated ignimbrite sample and iron oxide-coated ignimbrite sample.

Chemical Element	Uncoated Ignimbrite Concentration ($g{\cdot}kg^{-1}$)	Iron Oxide-Coated Ignimbrite Concentration ($g{\cdot}kg^{-1}$)
Ag	0.134 ± 0.14	0.114 ± 0.32
Ba	0.941 ± 0.11	0.561 ± 0.07
Cu	1.727 ± 0.21	1.042 ± 0.53
Fe	0.119 ± 0.14	17.729 ± 0.09
K	12.929 ± 0.13	13.222 ± 0.14
Li	0.002 ± 0.11	0.004 ± 0.33
Mg	3.430 ± 0.09	1.961 ± 0.20
Mo	2.444 ± 0.07	3.513 ± 0.17
Na	21.009 ± 0.11	56.773 ± 0.11
Sr	0.755 ± 0.17	0.450 ± 0.34
Ti	11.959 ± 0.21	9.661 ± 0.13

3.2. Ignimbrite Modification by Coating with Iron Oxides

A 25 g ignimbrite sample was coated with iron oxides, a product made from ferric salt precipitate. These oxides appear in crystalline forms such as goethite (α-FeOOH), hematite (α-Fe_2O_3), ferrihydrite ($Fe_5HO_8{\cdot}4H_2O$), and lepidocrocite (γ-FeOOH), which differ from each other in chemical structure, composition, and physical characteristics [32,33].

$Fe(OH)_3$ formation in the ignimbrite immersion solution facilitates dehydration and dehydroxylation reactions during heating that generates α-FeOOH and α-Fe_2O_3 as a final product—Equation (10). Possible reactions that take place are detailed below:

$$Fe(NO_3)_3 \rightarrow Fe^{3+} + 3\ NO^-{}_3 \quad (8)$$

$$Fe(NO_3)_3 + 3\ NaOH \rightarrow Fe(OH)_3 + 3\ NaNO_3 \quad (9)$$

$$2\ Fe(OH)_3\ \Delta\rightarrow 2\ aFeOOH + 2\ H_2O\ \Delta\rightarrow aFe_2O_3 + 3\ H_2O \quad (10)$$

Along with their structures, goethite and hematite present isostructures of other metal oxides: diaspore (α-AlOOH) for goethite and corundum (α-Al_2O_3) for hematite [25]. Furthermore, this crystalline oxide form presents hexagonal close-packed (hcp) structures, implying a cation enclosed by anions that form a hexagonal structure. In goethite, each Fe atom is surrounded by three O^{-2} and three OH^- to produce $FeO_3(OH)_3$ octahedra. In the hematite case, six O atoms surround each Fe atom octahedrally [34,35].

A possible reaction mechanism is proposed considering iron oxide structures formed during the ignimbrite coating process and its mineralogical composition (Scheme 1).

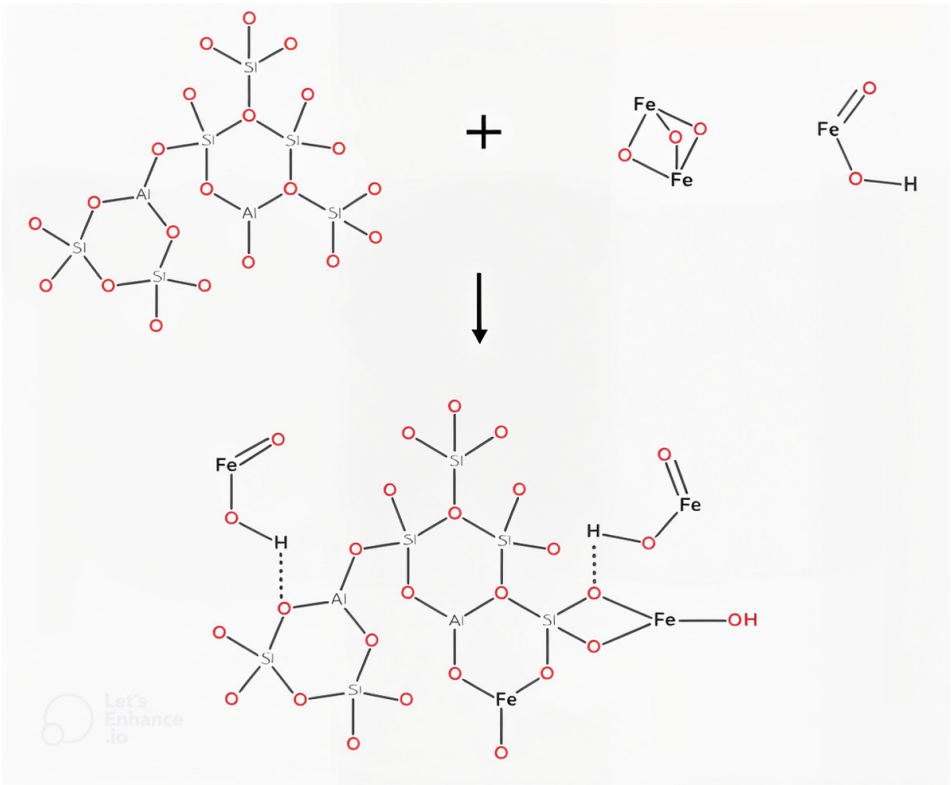

Scheme 1. A possible ignimbrite modification mechanism is by coating it with iron oxides.

Since goethite and hematite's specific surface areas are in the 8–200 $m^2 \cdot g^{-1}$ and 2–90 $m^2 \cdot g^{-1}$ ranges, respectively [34], it is assumed that the coated ignimbrite has a specific surface area in the same range.

At the end of ignimbrite's iron oxide coating process, an obvious change in its color was noticed, changing to a reddish-orange tone. This fact constituted physical proof of the modification's success. Furthermore, a 0.119 to 17.729 $g \cdot kg^{-1}$ increase in Fe concentration was evidenced, so a successful coating was deduced. On the other hand, a Na concentration increase was observed, which can be explained by the $NaNO_3$ formation in the coating solution as a reaction product carried out during this process.

Compared to other studies utilizing several natural or modified materials such as zeolites, activated carbon, or silica composites [36–39], iron oxide-coated ignimbrite demonstrates a competitive adsorption capacity for arsenic removal. This makes it a promising material, particularly due to its availability, its low cost, and the ease with which it can be modified. While materials like activated carbon may have higher adsorption capacities, ignimbrite offers significant advantages in terms of sustainability and local accessibility, making it a viable option for regions with high arsenic contamination. Additionally, the research indicates that modifying ignimbrite substantially enhances its efficiency, outperforming previous studies that used unmodified natural materials, as reported by Huayna et al. [40].

3.3. As(V) Removal by Iron Oxide-Coated Ignimbrite and As(V) Adsorption Capacity

3.3.1. Iron Oxide-Coated Ignimbrite Adsorbent Mass Effect

As(V) removal ranged from 24.39% ± 0.17% to 96.01% ± 0.11% within the tested adsorbent mass range of 0.025 g to 0.35 g (Figure 1). This trend can be attributed to the increased surface area of the adsorbent in contact with the As(V) solution. However, the adsorption capacity decreased from 9.78 $mg \cdot g^{-1}$ ± 0.02 $mg \cdot g^{-1}$, with a standard deviation of ±0.07 $mg \cdot g^{-1}$, to 3.19 $mg \cdot g^{-1}$ ± 0.09 $mg \cdot g^{-1}$, with a standard deviation of ±0.11 $mg \cdot g^{-1}$, across the same mass range, indicating that adsorption may be constrained

by the availability of active particles on the adsorbent surface. However, it is important to highlight that the percentage removal is an extensive variable that is directly dependent on the amount of adsorbent used. The observed reduction in arsenic adsorption capacity can be explained by the increased availability of adsorption sites, which requires a larger quantity of adsorbate to achieve saturation of the adsorbent. Additionally, no evidence of multilayer adsorption phenomena was observed under the experimental conditions tested. Based on these findings, an adsorbent mass of 0.15 g was selected for subsequent experiments.

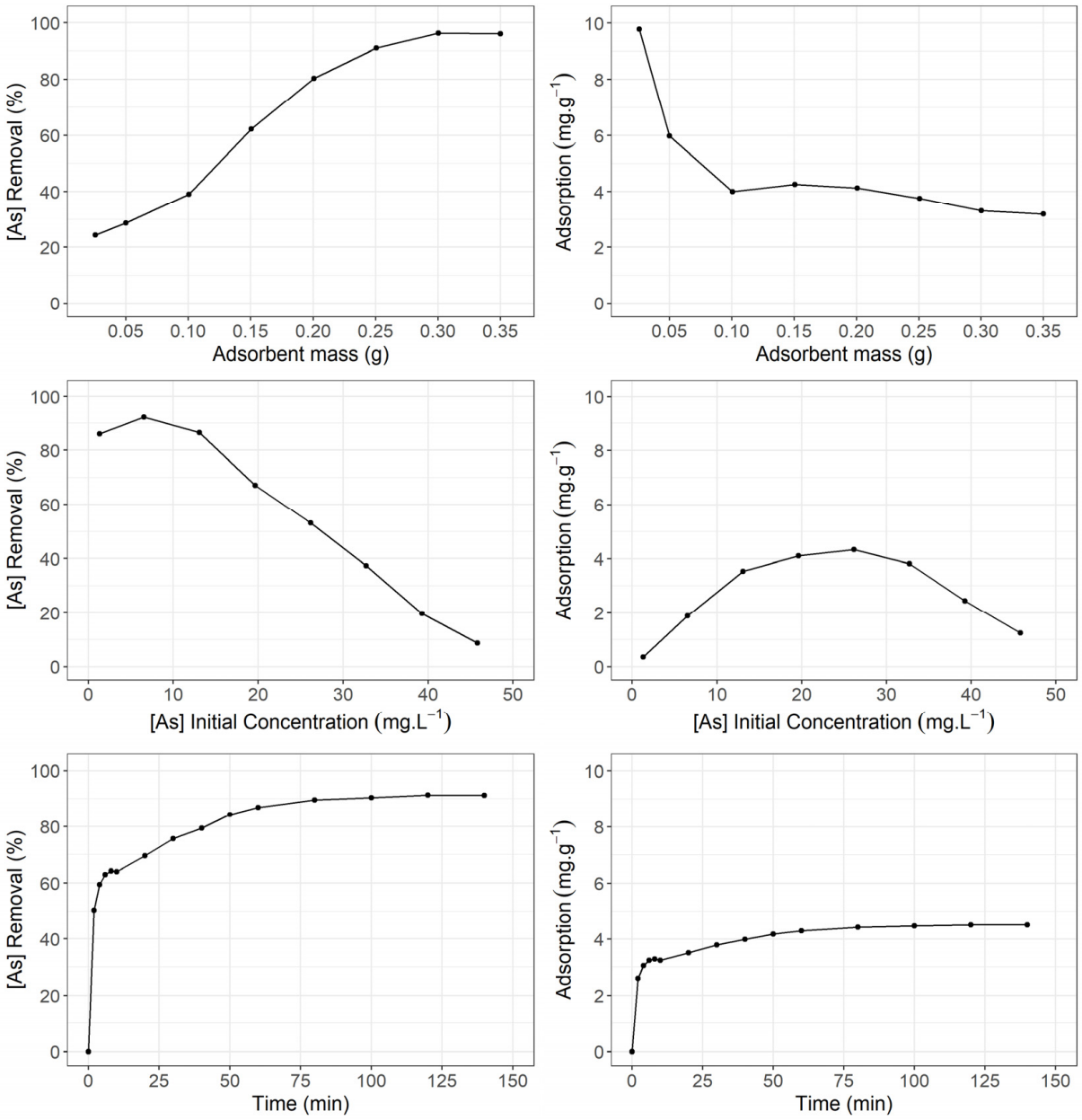

Figure 1. As(V) removal percentage and adsorption capacity (mg·g^{-1}) concerning adsorbent mass (g), initial As(V) concentration (mg·L^{-1}), and time (min). The experimental parameters presented in the figure include the adsorbent mass (ranging from 0.05 g to 0.35 g), the initial As(V) concentration (10 mg·L^{-1} to 40 mg·L^{-1}), and the contact time (0 to 120 min). These parameters were systematically varied to evaluate their impact on As(V) removal and the adsorption capacity of the material, providing a comprehensive assessment of the adsorbent's performance under different experimental conditions.

The results indicate that the adsorption efficiency of As(V) improves with optimized parameters such as adsorbent mass, initial concentration, and contact time. Consistent with previous studies, modifications to the adsorbent, such as coating chabazite with N-methylene aniline, enhance As(V) removal capacity by facilitating interactions with ions. Additionally, the rapid attainment of equilibrium suggests a high mass transfer rate. Temperature further enhances adsorption efficiency, aligning with findings from earlier research [41]. However, potential interferences from competing ions should be considered, as they may limit the adsorbent's effectiveness in practical applications.

Similar to the study on radionuclide sorption using a silica/olive peel nanocomposite [42], our research explores the efficiency of a modified adsorbent for arsenic (As) removal. Both studies demonstrate that combining natural materials significantly enhances adsorption capacity. Despite targeting different pollutants, the observed trends in adsorption efficiency and the influence of parameters such as pH and temperature are comparable, underscoring the potential of modified adsorbents for effective pollutant removal across various applications.

3.3.2. As(V) Ion Concentration Effect

A 2 h period assay at 293 K ± 1 K was performed to evaluate the As(V) concentration effect on its removal percentage and adsorption capacity, using 0.15 g of adsorbent. As(V) removal percentage showed a slight increase for As(V) concentrations between 1 $mg{\cdot}L^{-1}$ ± 0.02 $mg{\cdot}g^{-1}$, with a standard deviation of ±0.11 $mg{\cdot}g^{-1}$ and 6.5 $mg{\cdot}L^{-1}$ ± 0.09 $mg{\cdot}g^{-1}$, with a standard deviation of ±0.14 $mg{\cdot}g^{-1}$, where it decreased from 90% ± 0.16% to 8.6% ± 0.03% at a 45.8 $mg{\cdot}L^{-1}$ As(V) initial concentration (Figure 1).This finding may be due to the limited surface area of the modified ignimbrite particles that adsorb As(V) ions in the solution. On the other hand, in terms of adsorption capacity, an adsorption peak of 4.33 $mg{\cdot}g^{-1}$ ± 0.15 $mg{\cdot}g^{-1}$, with a standard deviation of ±0.08 $mg{\cdot}g^{-1}$, occurs at a 26.2 $mg{\cdot}L^{-1}$ As(V) initial concentration. With these results, it was decided to use 15 $mg{\cdot}L^{-1}$ As(V) stock solutions for subsequent investigations.

3.3.3. Contact Time Effect

Next, 50 mL of a 15 $mg{\cdot}L^{-1}$ As(V) stock solution and 0.15 g of adsorbent were used at 293 K ± 1 K temperature to determine the contact time effect in As(V) removal and adsorption capacity. The measurements were carried out at different periods for 140 min. However, a 60 min contact period was sufficient to achieve equilibrium (Figure 1). These results suggest a two-step mechanism: a very fast As(V) initial adsorption in the first 10 min, followed by a slower period until equilibrium. Over 85% of As(V) removal occurred in the first 60 min. The maximum removal percentage (91.28% ± 0.43%) was reached at 120 min of contact time.

3.3.4. Temperature Effect

Additionally, 50 mL of a 15 $mg{\cdot}L^{-1}$ As(V) stock solution and 0.15 g of adsorbent were used to compare 283 K, 293 K, and 303 K ± 1 K temperature effects. The highest removal percentage (91.18%) was registered at 293 K (Figure 2). Likewise, at 293 K, the highest adsorption capacity value (4.50 $mg{\cdot}g^{-1}$ ± 0.13 $mg{\cdot}g^{-1}$, with a standard deviation of ±0.05 $mg{\cdot}g^{-1}$) was reached. It is noted that, to optimize the process, it is advisable to maintain a temperature of 293 K ± 1 K.

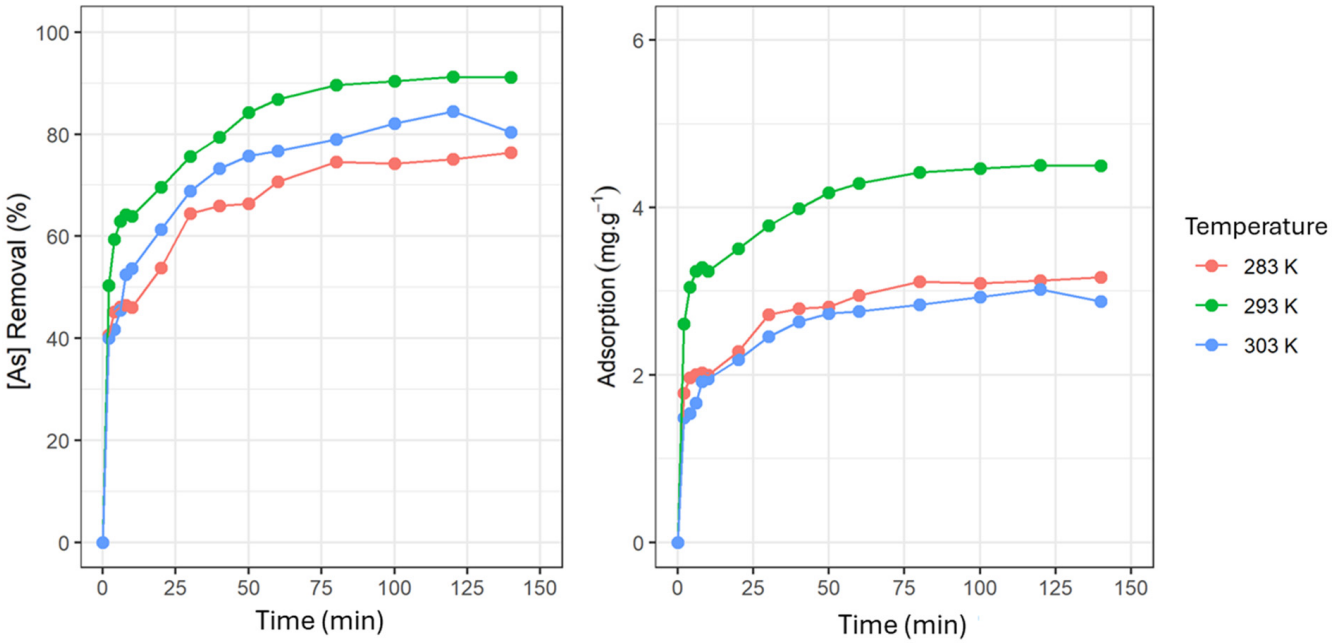

Figure 2. As(V) removal percentage and adsorption capacity ($mg \cdot g^{-1}$) concerning time at 283, 293, and 303 K. The experimental parameters in this figure include temperature (283 K, 293 K, and 303 K) and contact time (0 to 150 min). These parameters were analyzed to investigate As(V) removal (in percentage) and adsorption capacity (in $mg \cdot g^{-1}$) as functions of time at different temperatures. The curves illustrate how adsorption efficiency evolves over time and varies with temperature, highlighting the differences in sorption behavior under the three evaluated thermal conditions.

3.4. Adsorption Balance

Langmuir's and Freundlich's isotherm models were used to elucidate the adsorption mechanism and the interaction between As(V) and the adsorbent under study [29,30]. The test took place using a 15 g/47 mL adsorbent concentration for 120 min at 293 K ± 1 K. Isotherm constants and correlation coefficients were obtained (Table 2). These results showed that the Langmuir model presented a higher correlation coefficient (R^2 = 0.9855) than the Freundlich model (R^2 = 0.7268) (Figure 3), indicating that the experimental data best fit a monolayer-type adsorption model. According to Langmuir's isotherm, the maximum adsorption capacity 4.84 $mg \cdot g^{-1}$ ± 0.12 $mg \cdot g^{-1}$ of As(V), with a standard deviation of ±0.05 $mg \cdot g^{-1}$, a close value to the experimental one (4.33 $mg \cdot g^{-1}$ ± 0.09 $mg \cdot g^{-1}$ of As(V), with a standard deviation of ±0.11 $mg \cdot g^{-1}$) found in a previous study [43].

Table 2. Langmuir's and Freundlich's isotherm constants for As(V) adsorption by iron oxide-coated ignimbrite and their correlation coefficients.

Adsorption Isotherm Model	Temperature 293 K
Langmuir's isotherm	
q_m ($mg \cdot g^{-1}$)	4.84
K_L ($L \cdot mg^{-1}$)	0.7754
R^2	0.9855
Freundlich's isotherm	
n	1.870
K_f ($mg \cdot g^{-1}(mg \cdot L^{-1})^{-1/n}$)	1.5871
R^2	0.7268

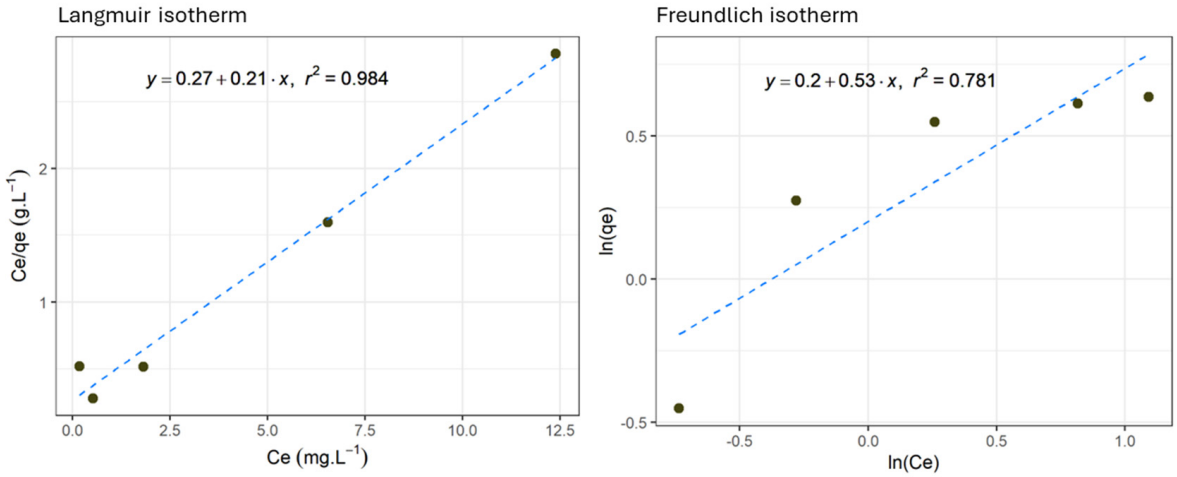

Figure 3. As(V) adsorption isotherms at 293 K according to Langmuir's and Freundlich's models. The experimental parameters in this figure correspond to the Langmuir and Freundlich isotherms for As(V) adsorption using the iron oxide-coated adsorbent. The Langmuir isotherm, shown in the graph on the left, illustrates the relationship between Ce (equilibrium concentration in mg·L^{-1}) and C_e/q_e (the ratio of the equilibrium concentration to the amount adsorbed). The correlation coefficient (R^2) for Langmuir is 0.984, indicating an excellent fit of the model to the experimental data. The Freundlich isotherm, presented in the graph on the right, shows the relationship between ln(C_e) and ln(q_e). With a lower correlation coefficient (R^2 = 0.781), the Freundlich model demonstrates a poorer fit to the experimental data than the Langmuir model.

Although the Freundlich model does not fit the experimental data and the Langmuir model, it is noteworthy that the n value falls within the range of 1–10. This indicates that the adsorption process is likely favorable under the studied conditions, suggesting a chemisorption process. Chemisorption, unlike physisorption, involves stronger chemical bonds between the adsorbent and adsorbate, which can explain the higher efficiency of the adsorption. These findings align with studies by Hsu et al. [44] and Thirunavukkarasu et al. [25], where similar n values were also associated with favorable adsorption processes.

3.5. Adsorption Kinetics

Experimental qe values obtained in the kinetic study showed that the highest adsorption capacity (4.44 mg·g^{-1} ± 0.03 mg·g^{-1}, with a standard deviation of ±0.05 mg·g^{-1}) occurred at 293 K, followed by 3.09 mg·g^{-1} ± 0.25 mg·g^{-1}, with a standard deviation of ±0.19 mg·g^{-1}, at 283 K, and 2.89 mg·g^{-1} ± 0.40 mg·g^{-1}, with a standard deviation of ±0.17 mg·g^{-1}, at 303 K. The correlation coefficients indicated that, for all three temperatures studied, the pseudo-first-order model best fit the experimental data (Figure 4). It was also observed that the R^2 value increases as the system temperature increases (0.9685 < 0.9736 < 0.9917). This same event happened with the speed value constant k_1, while the calculated q_e values are below the experimental q_e values. In contrast, the R^2 values for the pseudo-second-order model showed that, at 293 K, the experimental data fit this model better than at 283 K and 303 K (Figure 4). Likewise, speed constant k_2 showed similar values for 283 K and 303 K temperatures (0.0698 and 0.0796, respectively). On the other hand, the speed value constant k_2 decreases (0.0390) at 293 K. It was also evidenced that calculated q_e values in the pseudo-second-order model were notably closer to the experimental q_e values than those in the pseudo-first-order model, particularly at 283 K and 303 K.

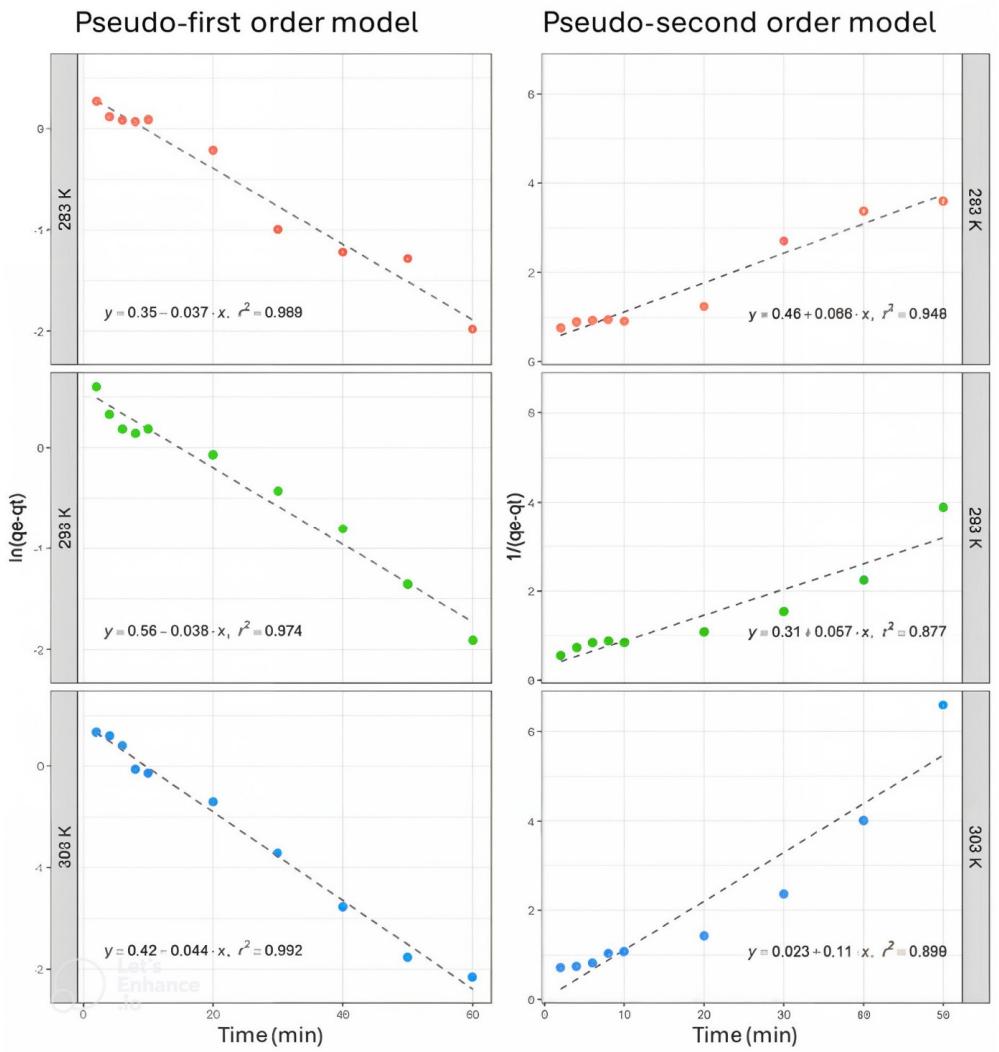

Figure 4. As(V) adsorption kinetics using 0.15 g/50 mL adsorbent concentration at 283, 293, and 303 K. The experimental parameters in this figure correspond to the kinetics of As(V) adsorption using an adsorbent concentration of 0.15 g/50 mL at three different temperatures: 283 K, 293 K, and 303 K. These experiments illustrate how As(V) removal (in percentage) and adsorption capacity (in $mg \cdot g^{-1}$) vary over time under different thermal conditions. The graphs show the As(V) adsorption progression for each temperature as a function of elapsed time, highlighting the process's adsorption behavior and thermal dependence.

Based on the correlation coefficients, the experimental data at 293 K fit best with the pseudo-first-order model, indicating that this model more accurately describes the adsorption kinetics of As(V) on iron oxide-coated ignimbrite. However, the results also suggest that, while the pseudo-first-order model effectively captures the adsorption rate, the pseudo-second-order model better represents the total adsorption capacity. These findings imply that the adsorption process of As(V) involves a mechanism combining the gradual occupation of adsorption sites with the simultaneous effects of external and internal diffusion throughout the entire adsorption process [34,35].

Pseudo-first-order and pseudo-second-order speed constants k_1 and k_2, calculated q_e value, and the corresponding correlation coefficient value R^2 for both mathematical models are summarized in Table 3.

Table 3. Pseudo-first-order and pseudo-second-order kinetic parameters for As(V) by iron oxide-coated ignimbrite.

Temperature (K)	283	293	303
As(V) initial concentrations ($mg \cdot L^{-1}$)	12.147	14.765	10.617
Pseudo-first order			
Experimental q_e ($mg \cdot g^{-1}$)	3.09	4.44	2.89
Calculated q_e ($mg \cdot g^{-1}$)	1.42	1.76	1.51
k_1 ($1 \cdot min^{-1}$)	0.0372	0.0381	0.0433
R^2	0.9685	0.9736	0.9917
Pseudo-second order			
Experimental q_e ($mg \cdot g^{-1}$)	3.09	4.44	2.89
Calculated q_e ($mg \cdot g^{-1}$)	2.37	2.01	3.06
k_2 ($g \cdot mg^{-1} \cdot min^{-1}$)	0.0698	0.0390	0.0796
R^2	0.9242	0.9473	0.9242

3.6. Adsorption Mechanism

The surface complex formation process is the most widely accepted mechanism for arsenic adsorption by iron oxides, although it is not completely clarified [25,44,45]. The present research suggests a possible mechanism based on the goethite and hematite structure found on the modified ignimbrite surface.

During kinetic studies, the pH of the $Na_2HAsO_4 \cdot 7H_2O$ solution in contact with the adsorbent was measured. The pH value registered was 3.8 at the beginning of the adsorption process and 3.7 after the first hour. This last value remained constant until the end of the study, at 2 h 20 min.

Arsenate in an aqueous medium can exist in four forms: H_3AsO_4, $H_2AsO_4^-$, $HAsO_4^{-2}$, and AsO_4^{-3}. According to arsenic acid *pKa* values, the predominant species at a pH of 4, the registered one, is $H_2AsO_4^-$, so it is assumed that, under this ionic form, As(V) adsorption by iron oxide-coated ignimbrite occurs.

As proposed in Scheme 2, crystalline structures such as goethite and hematite cover the modified ignimbrite surface. Thus, hydroxyl groups would cover the entire surface of the adsorbent particles, allowing them to attract anions in acidic solutions by positively charging the adsorbent surface. However, this property could be lost as the solution pH increased.

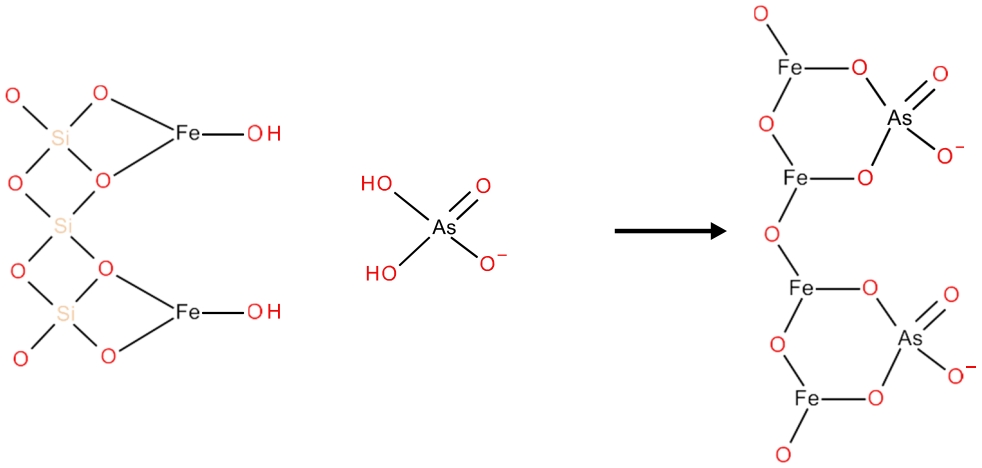

Scheme 2. Arsenic(V) is a possible adsorption mechanism by iron oxide-coated ignimbrite.

As shown in Scheme 2, As(V) adsorption would be due to complex formation on the adsorbent surface by ligand exchange between the surface hydroxyl groups of the

modified ignimbrite and the protons of $H_2AsO_4^-$. This process could also involve the adsorbent surface deprotonation, forming inner-sphere surface complexes [46]. According to the proposed mechanism, from a geometric point of view, it is suggested that the AsO_4 tetrahedral structure would join the goethite octahedral structure (FeO_6), forming binuclear bidentate complexes as a result of sharing corners between two O atoms of AsO_4 and a pair of edge-sharing FeO_6 octahedra (^{2}C in Scheme 3). Likewise, Sherman and Randall [47] pointed out that monodentate complex formation (^{1}V in Scheme 3) and mononuclear bidentate complexes are feasible due to sharing edges between an AsO_4 tetrahedron and the free edge of a FeO_6 octahedron (^{2}E in Scheme 3).

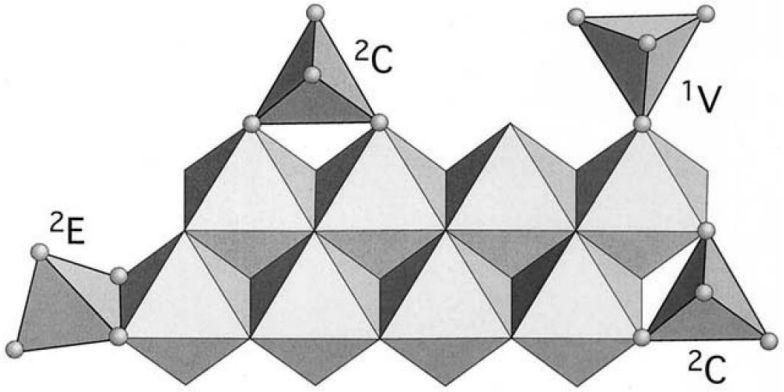

Scheme 3. AsO_4 possible surface complexes on goethite.

To corroborate the As(V) adsorption by the iron oxide-coated ignimbrite, an ICP–OES analysis was carried out on an adsorbent sample used in one of the kinetic tests. It was determined that arsenic presence in the modified ignimbrite at a 2203 g As(V) per kg of ignimbrite concentration could confirm covalent bond formation between them and, therefore, iron oxide-coated ignimbrite efficiency as a potential adsorbent.

4. Conclusions

This study demonstrates the successful modification of ignimbrite through the proposed iron oxide-coating procedure, confirmed by ICP–OES analysis, which revealed an iron concentration of 17.73 $g \cdot kg^{-1}$ in the modified material. Additionally, a linear, precise, and accurate voltammetric technique was developed to determine As(V) concentration in aqueous media quantitatively. Optimal adsorption parameters were identified, including an adsorbent concentration of 0.15 g/50 mL, a minimum contact time of 60 min, and a temperature of 293 K $\pm$ 1 K, achieving an adsorption capacity of 15 $mg \cdot L^{-1}$ of As(V). The formation of inner-sphere surface complexes was confirmed as the primary adsorption mechanism for As(V). The efficiency of the iron oxide-coated ignimbrite was further validated, with an arsenic concentration of 2.203 $g \cdot kg^{-1}$ detected in the adsorbent at the end of the adsorption process. Kinetic analysis revealed that the pseudo-first-order model was the most suitable for describing the adsorption under most experimental conditions. However, the pseudo-second-order model provided a good fit at specific temperatures. These findings highlight the feasibility and effectiveness of the developed adsorbent for As(V) removal, demonstrating its potential for environmental and technological applications.

Further studies evaluating the individual components (ignimbrite and iron oxide) separately are recommended to better understand their individual contributions to adsorption. Such investigations could provide valuable insights to optimize the modified material's effectiveness for arsenate As(V) removal.

Author Contributions: Writing—original draft and Methodology, L.D.V.-A.; Supervision, A.C.-C.; Writing—review and editing, R.S.-A. and J.-P.C.; Resources, J.A.V.-S. All authors have read and agreed to the published version of the manuscript.

Funding: This research was funded by the INIA project CUI 2487112 "Mejoramiento de los servicios de investigación y transferencia tecnológica en el manejo y recuperación de suelos agrícolas degradados y aguas para riego en la pequeña y mediana agricultura en los departamentos de Lima, Áncash, San Martín, Cajamarca, Lambayeque, Junín, Ayacucho, Arequipa, Puno y Ucayali".

Data Availability Statement: The raw data supporting the conclusions of this article will be made available by the authors on request.

Conflicts of Interest: The authors declare no conflicts of interest.

References

1. Kumar, V.; Parihar, R.D.; Sharma, A.; Bakshi, P.; Singh Sidhu, G.P.; Bali, A.S.; Karaouzas, I.; Bhardwaj, R.; Thukral, A.K.; Gyasi-Agyei, Y.; et al. Global Evaluation of Heavy Metal Content in Surface Water Bodies: A Meta-Analysis Using Heavy Metal Pollution Indices and Multivariate Statistical Analyses. *Chemosphere* **2019**, *236*, 124364. [CrossRef] [PubMed]
2. Zhang, Z.; Wang, J.J.; Ali, A.; DeLaune, R.D. Heavy Metals and Metalloid Contamination in Louisiana Lake Pontchartrain Estuary along I-10 Bridge. *Transp. Res. Part D Transp. Environ.* **2016**, *44*, 66–77. [CrossRef]
3. Monteiro De Oliveira, E.C.; Caixeta, E.S.; Santos, V.S.V.; Pereira, B.B. Arsenic Exposure from Groundwater: Environmental Contamination, Human Health Effects, and Sustainable Solutions. *J. Toxicol. Environ. Health Part B* **2021**, *24*, 119–135. [CrossRef]
4. Lamm, S.H.; Boroje, I.J.; Ferdosi, H.; Ahn, J. A Review of Low-Dose Arsenic Risks and Human Cancers. *Toxicology* **2021**, *456*, 152768. [CrossRef]
5. Palma-Lara, I.; Martínez-Castillo, M.; Quintana-Pérez, J.C.; Arellano-Mendoza, M.G.; Tamay-Cach, F.; Valenzuela-Limón, O.L.; García-Montalvo, E.A.; Hernández-Zavala, A. Arsenic Exposure: A Public Health Problem Leading to Several Cancers. *Regul. Toxicol. Pharmacol.* **2020**, *110*, 104539. [CrossRef] [PubMed]
6. Sharma, A.; Kumar, S. Arsenic Exposure with Reference to Neurological Impairment: An Overview. *Rev. Environ. Health* **2019**, *34*, 403–414. [CrossRef] [PubMed]
7. Signes-Pastor, A.J.; Vioque, J.; Navarrete-Muñoz, E.M.; Carey, M.; García-Villarino, M.; Fernández-Somoano, A.; Tardón, A.; Santa-Marina, L.; Irizar, A.; Casas, M.; et al. Inorganic Arsenic Exposure and Neuropsychological Development of Children of 4–5 Years of Age Living in Spain. *Environ. Res.* **2019**, *174*, 135–142. [CrossRef] [PubMed]
8. Alka, S.; Shahir, S.; Ibrahim, N.; Ndejiko, M.J.; Vo, D.V.N.; Manan, F.A. Arsenic Removal Technologies and Future Trends: A Mini Review. *J. Clean. Prod.* **2021**, *278*, 123805. [CrossRef]
9. Terracciano, A.; Ge, J.; Meng, X. A Comprehensive Study of Treatment of Arsenic in Water Combining Oxidation, Coagulation, and Filtration. *J. Environ. Sci.* **2015**, *36*, 178–180. [CrossRef] [PubMed]
10. Ungureanu, G.; Santos, S.; Boaventura, R.; Botelho, C. Arsenic and Antimony in Water and Wastewater: Overview of Removal Techniques with Special Reference to Latest Advances in Adsorption. *J. Environ. Manag.* **2015**, *151*, 326–342. [CrossRef]
11. Wang, A.; Zhou, K.; Zhang, X.; Zhou, D.; Peng, C.; Chen, W. Arsenic Removal from Highly-Acidic Wastewater with High Arsenic Content by Copper-Chloride Synergistic Reduction. *Chemosphere* **2020**, *238*, 124675. [CrossRef] [PubMed]
12. Asere, T.G.; Stevens, C.V.; Du Laing, G. Use of (Modified) Natural Adsorbents for Arsenic Remediation: A Review. *Sci. Total Environ.* **2019**, *676*, 706–720. [CrossRef]
13. Hao, L.; Liu, M.; Wang, N.; Li, G. A Critical Review on Arsenic Removal from Water Using Iron-Based Adsorbents. *RSC Adv.* **2018**, *8*, 39545–39560. [CrossRef]
14. Mohan, D.; Pittman, C.U. Arsenic Removal from Water/Wastewater Using Adsorbents—A Critical Review. *J. Hazard. Mater.* **2007**, *142*, 1–53. [CrossRef] [PubMed]
15. Yılmaz, Ş.; Zengin, A.; Şahan, T. A Novel Material Poly(N-Acryloyl-L-Serine)-Brush Grafted Kaolin for Efficient Elimination of Malachite Green Dye from Aqueous Environments. *Colloids Surf. A Physicochem. Eng. Asp.* **2020**, *601*, 125041. [CrossRef]
16. Yılmaz, Ş.; Zengin, A.; Şahan, T.; Zorer, Ö.S. Utilization of a Novel Polymer–Clay Material for High Elimination of Hazardous Radioactive Contamination Uranium(VI) from Aqueous Environments. *Environ. Technol. Innov.* **2021**, *23*, 101631. [CrossRef]
17. Yılmaz, Ş.; Zengin, A.; Şahan, T.; Gübbük, İ.H. Efficient Removal of 2,4-Dichlorophenoxyacetic Acid from Aqueous Medium Using Polydopamine/Polyacrylamide Co-Deposited Magnetic Sporopollenin and Optimization with Response Surface Methodology Approach. *J. Polym. Environ.* **2023**, *31*, 36–49. [CrossRef]
18. Consideraciones y Reflexiones En Torno a La Ruta Del Sillar En Arequipa—Instituto De Investigaciones Del Patrimonio Cultural. Available online: https://patrimonioculturalperu.com/2019/07/04/consideraciones-y-reflexiones-en-torno-a-la-ruta-del-sillar-en-arequipa/ (accessed on 11 November 2024).

19. Lebti, P.P.; Thouret, J.C.; Wörner, G.; Fornari, M. Neogene and Quaternary Ignimbrites in the Area of Arequipa, Southern Peru: Stratigraphical and Petrological Correlations. *J. Volcanol. Geotherm. Res.* **2006**, *154*, 251–275. [CrossRef]
20. Chowdhury, S.R.; Yanful, E.K.; Pratt, A.R. Arsenic Removal from Aqueous Solutions by Mixed Magnetite-Maghemite Nanoparticles. *Environ. Earth Sci.* **2011**, *64*, 411–423. [CrossRef]
21. Khan, J.; Lin, S.; Nizeyimana, J.C.; Wu, Y.; Wang, Q.; Liu, X. Removal of Copper Ions from Wastewater via Adsorption on Modified Hematite (α-Fe2O3) Iron Oxide Coated Sand. *J. Clean. Prod.* **2021**, *319*, 128687. [CrossRef]
22. Peter, K.T.; Myung, N.V.; Cwiertny, D.M. Surfactant-Assisted Fabrication of Porous Polymeric Nanofibers with Surface-Enriched Iron Oxide Nanoparticles: Composite Filtration Materials for Removal of Metal Cations. *Environ. Sci. Nano* **2018**, *5*, 669–681. [CrossRef]
23. Pearson, R.G. Hard and Soft Acids and Bases, HSAB, Part 1: Fundamental Principles. *J. Chem. Educ.* **1968**, *45*, 581. [CrossRef]
24. Schwertmann, U.; Cornell, R.M. *Iron Oxides in the Laboratory*, 2nd ed.; Completely Revised and Enlarged Edition; 2000; p. 204. Available online: https://www.wiley.com/en-au/Iron+Oxides+in+the+Laboratory:+Preparation+and+Characterization,+2nd,+Completely+Revised+and+Enlarged+Edition-p-9783527296699 (accessed on 15 November 2024).
25. Thirunavukkarasu, O.S.; Viraraghavan, T.; Subramanian, K.S. Arsenic Removal from Drinking Water Using Iron Oxide-Coated Sand. *Water Air Soil. Pollut.* **2003**, *142*, 95–111. [CrossRef]
26. Metodologías Analíticas Para La Determinación y Especiación de Arsénico En Aguas y Suelos.—CONICET. Available online: https://bicyt.conicet.gov.ar/fichas/produccion/1867068 (accessed on 14 November 2024).
27. He, Y.; Zheng, Y.; Locke, D.C. Cathodic Stripping Voltammetric Analysis of Arsenic Species in Environmental Water Samples. *Microchem. J.* **2007**, *85*, 265–269. [CrossRef]
28. Scheiber, L.; Ayora, C.; Vázquez-Suñé, E.; Cendón, D.I.; Soler, A.; Baquero, J.C. Origin of High Ammonium, Arsenic and Boron Concentrations in the Proximity of a Mine: Natural vs. Anthropogenic Processes. *Sci. Total Environ.* **2016**, *541*, 655–666. [CrossRef]
29. Hussain, C.M. Carbon Nanomaterials as Adsorbents for Environmental Analysis. In *Nanomaterials for Environmental Protection*; Wiley Blackwell 6: Hoboken, NJ, USA, 2015; pp. 217–236, ISSN 9781118496978. [CrossRef]
30. Srivastava, S.; Goyal, P. Biosorbents Used So Far. In *Environmental Science and Engineering*; Springer: Berlin/Heidelberg, Germany, 2010; pp. 51–52. [CrossRef]
31. Ho, Y.S.; Porter, J.F.; McKay, G. Equilibrium Isotherm Studies for the Sorption of Divalent Metal Ions onto Peat: Copper, Nickel and Lead Single Component Systems. *Water Air Soil. Pollut.* **2002**, *141*, 1–33. [CrossRef]
32. Malana, M.A.; Ijaz, S.; Ashiq, M.N. Removal of Various Dyes from Aqueous Media onto Polymeric Gels by Adsorption Process: Their Kinetics and Thermodynamics. *Desalination* **2010**, *263*, 249–257. [CrossRef]
33. Matouq, M.; Jildeh, N.; Qtaishat, M.; Hindiyeh, M.; Al Syouf, M.Q. The Adsorption Kinetics and Modeling for Heavy Metals Removal from Wastewater by Moringa Pods. *J. Environ. Chem. Eng.* **2015**, *3*, 775–784. [CrossRef]
34. Benjamin, M.M.; Sletten, R.S.; Bailey, R.P.; Bennett, T. Sorption and Filtration of Metals Using Iron-Oxide-Coated Sand. *Water Res.* **1996**, *30*, 2609–2620. [CrossRef]
35. Eisazadeh, A.; Eisazadeh, H.; Kassim, K.A. Removal of Pb(II) Using Polyaniline Composites and Iron Oxide Coated Natural Sand and Clay from Aqueous Solution. *Synth. Met.* **2013**, *171*, 56–61. [CrossRef]
36. Pillewan, P.; Mukherjee, S.; Meher, A.K.; Rayalu, S.; Bansiwal, A. Removal of Arsenic (III) and Arsenic(V) Using Copper Exchange Zeolite-a. *Environ. Prog. Sustain. Energy* **2014**, *33*, 1274–1282. [CrossRef]
37. Aremu, J.O.; Lay, M.; Glasgow, G. Kinetic and Isotherm Studies on Adsorption of Arsenic Using Silica Based Catalytic Media. *J. Water Process Eng.* **2019**, *32*, 100939. [CrossRef]
38. Arcibar-Orozco, J.A.; Josue, D.B.; Rios-Hurtado, J.C.; Rangel-Mendez, J.R. Influence of Iron Content, Surface Area and Charge Distribution in the Arsenic Removal by Activated Carbons. *Chem. Eng. J.* **2014**, *249*, 201–209. [CrossRef]
39. Heredia, A.; Gómez Avila, J.; Vinuesa, A.; Saux, C.; Mendoza, S.M.; Garay, F.; Crivello, M. Compared Arsenic Removal from Aqueous Solutions by Synthetic Mixed Oxides and Modified Natural Zeolites. *Adsorption* **2019**, *25*, 1425–1436. [CrossRef]
40. Huayna, G.; Laura, A.; Churata, R.; Lazo, L.; Guzmán, R.; Ramos, P.G.; Rodriguez, J.M. Synthesis and Characterization of a Photocatalytic Material from TiO2 Nanoparticles Supported on Zeolite Obtained from Ignimbrite Residue Used in Decolorization of Methyl Orange. *Appl. Sci.* **2024**, *14*, 3146. [CrossRef]
41. Metwally, S.S.; Attallah, M.F. Impact of Surface Modification of Chabazite on the Sorption of Iodine and Molybdenum Radioisotopes from Liquid Phase. *J. Mol. Liq.* **2019**, *290*, 111237. [CrossRef]
42. Attallah, M.F.; Rizk, S.E.; El Afifi, E.M. Efficient Removal of Iodine and Chromium as Anionic Species from Radioactive Liquid Waste Using Prepared Iron Oxide Nanofibers. *J. Radioanal. Nucl. Chem.* **2018**, *317*, 933–945. [CrossRef]
43. Ramón de los Santos, C.; Barajas Fernández, J.; Pérez Hernández, G.; Hernández Rivera, M.Á.; Díaz Flores, L.L. Adsorption of copper (II) and cadmium (II) in aqueous suspensions of biogenic nanostructured $CaCO_3$. *Boletín de la Sociedad Española de Cerámica y Vidrio* **2019**, *58*, 2–13. [CrossRef]
44. Hsu, J.C.; Lin, C.J.; Liao, C.H.; Chen, S.T. Removal of As(V) and As(III) by Reclaimed Iron-Oxide Coated Sands. *J. Hazard. Mater.* **2008**, *153*, 817–826. [CrossRef]

45. Gupta, V.K.; Saini, V.K.; Jain, N. Adsorption of As(III) from Aqueous Solutions by Iron Oxide-Coated Sand. *J. Colloid. Interface Sci.* **2005**, *288*, 55–60. [CrossRef] [PubMed]
46. Yiacoumi, S.; Tien, C. *Kinetics of Metal Ion Adsorption from Aqueous Solutions*; Springer: Berlin/Heidelberg, Germany, 1995. [CrossRef]
47. Sherman, D.M.; Randall, S.R. Surface Complexation of Arsenic(V) to Iron(III) (Hydr)Oxides: Structural Mechanism from Ab Initio Molecular Geometries and EXAFS Spectroscopy. *Geochim. Cosmochim. Acta* **2003**, *67*, 4223–4230. [CrossRef]